

## ASYMPTOTIC REGIMES FOR DIFFRACTIVE SCATTERINGS AT ULTRAHIGH ENERGIES AND COULOMB INTERACTION

V.V. ANISOVICH, V.A. NIKONOV

*National Research Centre "Kurchatov Institute", Petersburg Nuclear Physics Institute, Gatchina  
188300, Russia*

J. NYIRI

*Institute for Particle and Nuclear Physics, Wigner RCP, Budapest 1121, Hungary*

Received Day Month Year

Revised Day Month Year

Comparative analysis of the interplay of hadron and Coulomb interactions in  $pp^\pm$  scattering amplitudes is performed for two extreme cases: for the asymptotic interaction of hadrons in black disk and resonant disk modes. The interactions are discussed in terms of the  $K$ -matrix function technique, the interference effects are estimated in the energy interval  $\sqrt{s} = 1 - 10^6$  TeV. In both cases the real part of the hadronic amplitude is concentrated on the boundary of the disks in the impact parameter space that causes a growth of interference effects with the energy increase. For the  $pp$  scattering at  $\sqrt{s} \sim 10$  TeV an interplay of the hadron and Coulomb interactions in the resonant disk modes is realized in a specific shoulder in  $d\sigma_{el}/d\mathbf{q}^2$  at  $\mathbf{q}^2 \sim 0.0025 - 0.0075$  GeV<sup>2</sup>.

PACS numbers: 13.85.Lg, 13.85.-t, 13.75.Cs, 14.20.Dh

### 1. Introduction

The analysis of the pre-LHC<sup>1-5</sup> and LHC<sup>6-9</sup> data for hadronic total cross sections and diffractive scattering cross sections points to a steady growth of the optical density in the impact parameter space,  $T(b, \ln s)$ , with increasing energy,  $\sqrt{s}$ . At LHC energy the profile function of the  $pp$ -scattering amplitude reaches the black disk limit at small  $b$ . Two extreme scenarios are possible at larger energies,  $\sqrt{s} \gtrsim 100$  TeV.

First, the profile function gets frozen in the black disk limit,  $T(b) \simeq 1$ , while the radius of the black disk,  $R_{black\ disk}$ , is increasing with  $\sqrt{s}$  providing  $\sigma_{tot} \sim \ln^2 s$ ,  $\sigma_{el} \sim \ln^2 s$ ,  $\sigma_{inel} \sim \ln^2 s$ . The black disk regime was studied in a number of papers, see refs.<sup>10-13</sup> and references therein.

In another scenario the profile function continues to grow at  $\sqrt{s} \gtrsim 100$  TeV approaching the maximal value,  $T(b) \simeq 2$ , that means the resonant disk mode. In this mode the disk radius,  $R_{resonant\ disk}$ , increases providing the  $\ln^2 s$ -growth of the total and elastic cross sections,  $\sigma_{tot} \sim \ln^2 s$ ,  $\sigma_{el} \sim \ln^2 s$ , but a slower increase of inelastic cross section,  $\sigma_{inel} \sim \ln s$ , see refs.<sup>14-16</sup>

Hadron physics at ultrahigh energies is a physics of large energy logarithms,  $\ln s \equiv \xi \gg 1$ ,<sup>17–19</sup> and increasing parton disks.<sup>20–24</sup> The black disk picture corresponds to the non-coherent parton interactions in hadron collisions. In the resonant disk mode the partons interact coherently thus providing a maximal cross section corresponding to the Froissart limit.<sup>25</sup>

In this paper, considering an interplay of hadron and Coulomb interactions, we concentrate our attention on the resonant disk mode; the corresponding consideration of the interplay in the black disk mode was performed in refs.<sup>26–28</sup>

For the hadronic scattering amplitude with switched off Coulomb interaction we write:

$$A^H(\mathbf{q}^2, \xi) = \int d^2b e^{i\mathbf{q}\cdot\mathbf{b}} T^H(b, \xi),$$

$$T^H(b, \xi) = 1 - \eta(b, \xi) \exp(2i\delta(b, \xi)) = \frac{-2iK^H(b, \xi)}{1 - iK^H(b, \xi)}, \quad (1)$$

where  $\xi = \ln s$  and  $b = |\mathbf{b}|$ . The complex function  $K^H(b, \xi)$  presents part of amplitude without rescatterings or with inelastic processes in the intermediate states only.

For the imaginary and real parts of the introduced functions we write<sup>26,27</sup> :

$$-iK^H(b, \xi) = K_{\Im}^H(b, \xi) - iK_{\Re}^H(b, \xi) \simeq K_{\Im}^H(b, \xi) - i\frac{\pi}{2} \frac{\partial K_{\Im}^H(b, \xi)}{\partial \xi}. \quad (2)$$

At the asymptotic regime the imaginary part of the amplitude is a generating function for the real part of the amplitude, the asymptotic equality  $[\sigma_{tot}(pp)/\sigma_{tot}(p\bar{p})]_{\sqrt{s} \rightarrow \infty} = 1$  is supposed for that, see refs.<sup>26,27</sup> for details. The total and diffractive cross sections read:

$$\sigma_{tot} = 2 \int d^2b T_{\Im}^H(b, \xi), \quad 4\pi \frac{d\sigma_{el}}{d\mathbf{q}^2} = (1 + \rho^2) \left| A_{\Im}^H(\mathbf{q}^2) \right|^2, \quad (3)$$

with the usual notation  $A_{\Re}^H(\mathbf{q}^2, \xi)/A_{\Im}^H(\mathbf{q}^2, \xi) = \rho(\mathbf{q}^2, \xi)$ . Taking into account that  $\rho^2$  is small ( $\rho^2 \sim 0.01$  and asymptotically  $\rho \sim 1/\ln s$ ) one can approximate:

$$\left| A_{\Im}^H(\mathbf{q}^2, \xi) \right| \simeq 2\pi^{\frac{1}{2}} \sqrt{\frac{d\sigma_{el}}{d\mathbf{q}^2}}, \quad (4)$$

Eq. (4) makes possible direct calculations of the real part of the scattering amplitude,  $A_{\Re}^H(\mathbf{q}^2, \xi)$ , on the basis of the energy dependence of the diffractive scattering cross section. The corresponding calculations were performed in ref.<sup>27</sup> using preLHC<sup>1–5</sup> and LHC<sup>6–9</sup> data. The results were extrapolated in the region  $\sqrt{s} = 10 - 10^6$  TeV using the black disk mode hypothesis for the asymptotic regime. The next step, an inclusion of the Coulomb interaction into consideration of the scattering amplitude, was made in refs.<sup>26,28</sup>

In Section 2 we calculate the real part of the hadronic amplitude in the resonant mode, the inclusion of the Coulomb interaction is performed in Section 3. A comparative analysis of results in the black disk and resonant disk modes is presented.

## 2. Resonant disk and K-matrix function

From the data it follows that both  $T^H(b)$  and  $-iK^H(b)$  are increasing with energy, being less than unity. If the eikonal mechanism does not quench the growth, both characteristics cross the black disk limit getting  $T^H(b) > 1$ ,  $-iK^H(b) > 1$ . If  $-iK^H(b) \rightarrow \infty$  at  $\ln s \rightarrow \infty$ , which corresponds to a growth caused by the supercritical pomeron ( $\Delta > 0$ ), the diffractive scattering process gets to the resonant disk mode.

For following the resonant disk switch-on we use the two-pomeron model with parameters providing the description of data at 1.8 TeV and 7 TeV, namely:

$$\begin{aligned}
 -iK^H(b) &= \int \frac{d^2q}{(2\pi)^2} \exp(-i\mathbf{qb}) \sum g^2 s^\Delta e^{-(a+\alpha\xi)q^2} \\
 &= \sum \frac{g^2}{4\pi(a+\alpha'\xi)} \exp\left[\Delta\xi - \frac{\mathbf{b}^2}{4(a+\alpha'\xi)}\right], \quad \xi = \ln \frac{s}{s_0}. \quad (5)
 \end{aligned}$$

The following parameters are found for the leading and the next-to-leading pomerons:

parameters	leading pole	next-to-leading
$\Delta$	0.20	0
$\alpha'_P$ [GeV <sup>-2</sup> ]	0.18	0.14
$a$ [GeV <sup>-2</sup> ]	6.67	2.22
$g^2$ [mb]	1.65	27.2
$s_0$ [GeV <sup>2</sup> ]	1	1

(6)

A similar description of the resonant disk mode but neglecting the real part of the amplitude was performed in ref.<sup>16</sup> The inclusion of the real part leads to some corrections of the parameters.

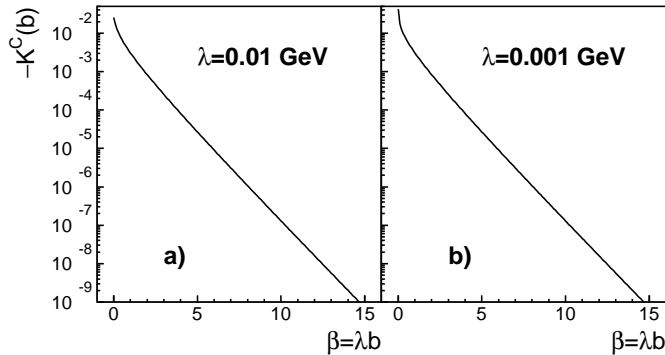


Fig. 1. The  $K$ -matrix function,  $-K^C(b)$ , for the pure Coulomb interaction in  $pp$  collision at different  $\lambda$ , we use  $\beta = \lambda b$  for abscissa with a)  $\lambda = 0.01$  GeV and b)  $\lambda = 0.001$  GeV.

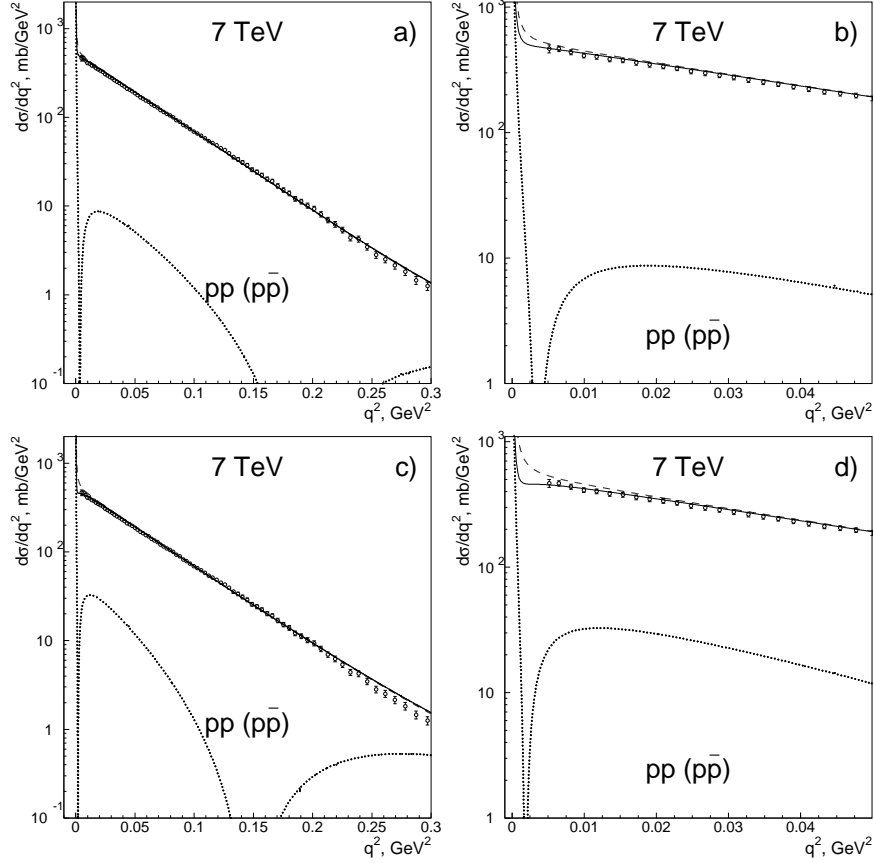


Fig. 2. Diffractive scattering cross section for  $pp$  at 7 TeV (TOTEM<sup>6</sup>) versus description with interplay of hadronic and Coulomb interactions (Eq. (10),  $\lambda=0.01$  GeV): figures (a,b) refer to the black disk mode, figures (c,d) refer to the resonant disk case; solid curves refer to  $pp$ , dashed ones to  $p\bar{p}$ . Dotted curves show a contribution of the real part in the  $pp$  scattering, the last term in Eq. (10).

### 3. Diffractive scattering amplitude at ultrahigh energy and Coulomb interaction

The interplay of hadronic and Coulomb interactions was studied in a set of papers, see<sup>29–35</sup> and references therein. In the region of ultrahigh energies and small  $\mathbf{q}^2$ , the  $K$ -matrix function technique allows to take into account directly the combined action of hadronic and Coulomb interactions ( $H + C$ ).

#### 3.1. Interplay of hadronic and Coulomb interactions in the $K$ -matrix function technique

We consider two types of scattering amplitudes and corresponding profile functions: the amplitude with combined interaction taken into account,  $A^{C+H}(\mathbf{q}^2, \xi)$

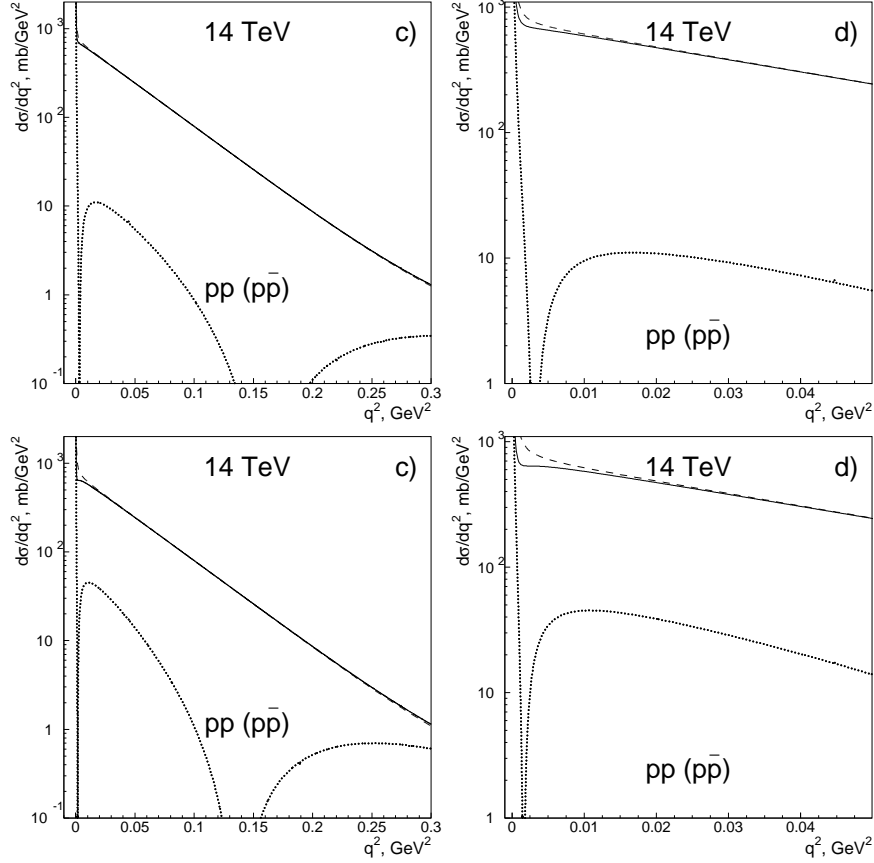


Fig. 3. Diffractive scattering cross sections for  $pp^\pm$  at 14 TeV (eq. (10),  $\lambda=0.01$  GeV): The figures (a,b) refer to the black disk mode and (c,d) to the resonant disk one; solid curves refer to  $pp$ , dashed ones to  $p\bar{p}$ . Dotted curves show a contribution of the real part in the  $pp$  scattering, the last term in Eq. (10).

and  $T^{C+H}(b, \xi)$ , and that with the switched-off Coulomb interaction,  $A^H(\mathbf{q}^2, \xi)$  and  $T^H(b, \xi)$ .

For the combined interaction profile function we write:

$$T^{C+H}(b, \xi) = \frac{-2iK^{C+H}(b, \xi)}{1 - iK^{C+H}(b, \xi)} = \frac{-2i(K^C(b) + K^H(b, \xi))}{1 - i(K^C(b) + K^H(b, \xi))}, \quad (7)$$

where the Coulomb interaction is written as:

$$A^C(\mathbf{q}^2) = \pm i f_1(\mathbf{q}^2) \frac{4\pi\alpha}{\mathbf{q}^2 + \lambda^2} f_2(\mathbf{q}^2),$$

$$-2iK^C(b) = \pm i \int \frac{d^2q}{(2\pi)^2} e^{i\mathbf{q}\mathbf{b}} f_1(\mathbf{q}^2) \frac{4\pi\alpha}{\mathbf{q}^2 + \lambda^2} f_2(\mathbf{q}^2). \quad (8)$$

Here  $\alpha = 1/137$ ; the upper/lower signs refer to the same/opposite charges of the colliding particles. The cutting parameter  $\lambda$ , which removes the infrared divergency,

can tend to zero in the final result for  $A^{C+H}(\mathbf{q}^2, \xi)$ . Colliding hadron form factors,  $f_1(\mathbf{q}^2)$  and  $f_2(\mathbf{q}^2)$ , guarantee the convergence of the integrals at  $\mathbf{q}^2 \rightarrow \infty$ ; for the  $pp^\pm$  collisions we use:

$$f_1(\mathbf{q}^2) = f_2(\mathbf{q}^2) = \frac{1}{(1 + \frac{\mathbf{q}^2}{0.71 \text{GeV}^2})^2}. \quad (9)$$

In Fig. 1 we show  $-K^C(b)$  for  $\lambda = 0.01$  GeV (Fig. 1a) and 0.001 GeV (Fig. 1b). At large  $b$  the  $K^C(b)$  is a scaling function in terms of  $\beta = \lambda b$ , the  $\beta$ -scaling gets broken at small  $\beta$ .

For a diffractive scattering cross section with Coulomb interaction taken into account we write now:

$$A^{H+C}(\mathbf{q}^2, \xi) = \int d^2b e^{i\mathbf{q}\mathbf{b}} T^{H+C}(b, \xi),$$

$$4\pi \frac{d\sigma_{el}}{d\mathbf{q}^2} = \left| A_{\Im}^{H+C}(\mathbf{q}^2) \right|^2 + \left| A_{\Re}^{H+C}(\mathbf{q}^2) \right|^2. \quad (10)$$

The diffractive scattering cross sections with Coulomb interaction taken into account are shown in Figs. 2,3 for  $\sqrt{s} = 7$  TeV (Fig. 2a-d) and for  $\sqrt{s} = 14$  TeV (Fig. 3a-d).

### 3.2. Interference of hadronic and Coulomb interactions

At the LHC energies ( $\sqrt{s} \sim 10$  TeV) the real part of the resonant disk amplitude demonstrates an essentially stronger peaking compared to that in the black disk mode, see Figs. 2, 3 for  $\left| A_{\Re}^{H+C}(\mathbf{q}^2) \right|^2$  and Figs. 4, 5 for  $K^{H+C}(b, \xi)$  and  $T^{H+C}(b, \xi)$ . For the resonant disk mode it results in a shoulder in the  $pp$  diffractive cross section  $\frac{d\sigma_{el}(\mathbf{q}^2)}{d\mathbf{q}^2}$  at  $\mathbf{q}^2 \sim 0.0025 - 0.0075$  GeV<sup>2</sup>, Figs. 2d, 3d. The shoulder is a qualitative attribute of the resonant disk picture in the  $pp$  scattering, and it means that a presence of the shoulder, or its absence, can serve as a sign for the disk modes.

### 3.3. Asymptotic regimes in the black disk and resonant disk modes

For the black disk mode the valuable asymptotic regime works starting at  $\sqrt{s} \gtrsim 10^2$  TeV. The real parts of  $K^{H+C}(b, \xi)$  and  $T^{H+C}(b, \xi)$  (see Figs. 4d, 5d) have peak shapes, with fixed maximal peak values  $\sim 0.12$  and  $\sim 0.10$ , respectively. At large  $b$  where the pure Coulomb interaction works ( $b > R_{disk\ radius}$ ) the  $K$ -matrix function (and the profile function) is negative for the  $pp$  scattering as it should be for particles with the same electric charge.

In the resonant disk mode the asymptotic value of the imaginary part of the amplitude reaches its maximal value,  $T_{\Im}^{H+C}(b, \xi) \simeq 2$  at  $b < R_{disk\ radius}$ , at  $\sqrt{s} \gtrsim 10^5$  TeV only. The maximal values of the real part continue to increase at  $\sqrt{s} \gtrsim 10^6$  TeV. The stable maximal values are reached at  $\sqrt{s} \gtrsim 10^{19}$  TeV where  $T_{\Re}^{H+C}(maximal) \simeq 0.6$ . Negative values of the real part of the  $pp$  scattering profile function,  $T_{\Re}^{H+C}(b, \xi) < 0$  at  $b > R_{disk\ radius}$ , are inherent to resonant disk mode as well.

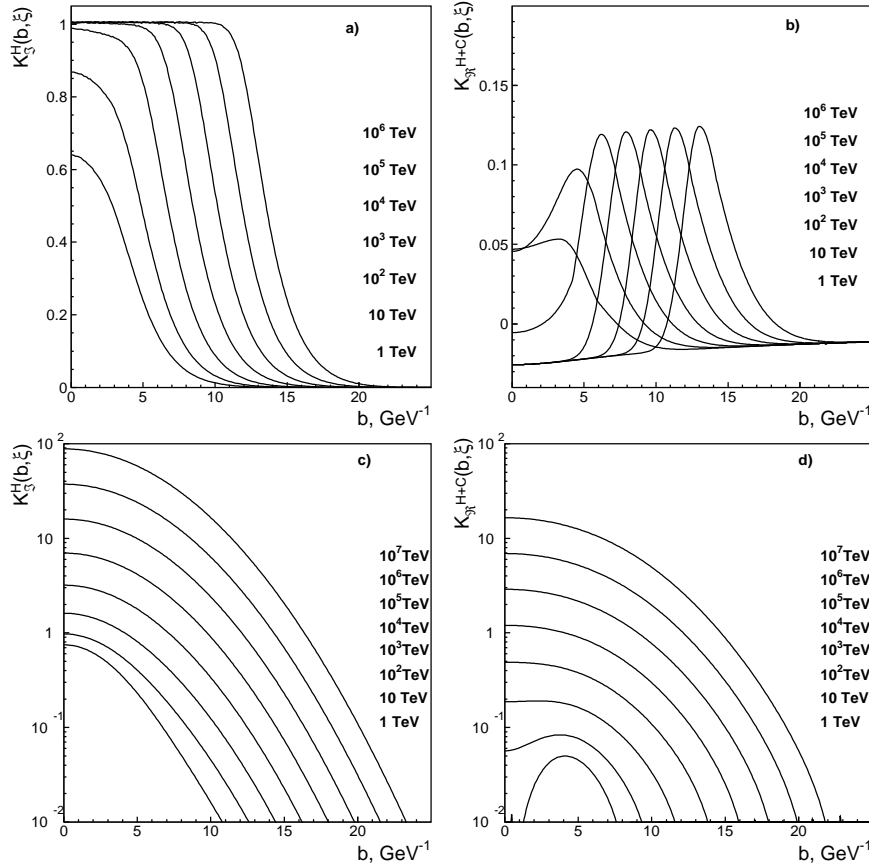


Fig. 4. K-matrix functions (imaginary and real parts) in the energy region  $\sqrt{s} = 1 - 10^6$  TeV; figures (a,b) refer to the black disk mode, (c,d) to the resonant disk mode.

#### 4. Conclusion

The problem of parton cloud structure of hadrons with ultrahigh energy is a subject of lively discussions.<sup>36–41</sup> A slow growth of the parton cloud radius with energy increase argues for a glueball origin of the parton clouds,<sup>22–24</sup> the glueball origin of the parton clouds leads to the universality of all hadron total cross sections.<sup>42</sup>

We study the asymptotic regime supposing for the parton clouds two different extreme modes: the black disk mode and resonant disk one. In the black disk mode the diffractive scattering occurs due to non-coherent parton interactions while the resonant disk scattering is the result of coherent interaction of partons with the same impact parameter  $b$ ; the resonant disk mode realizes the maximal growth of the amplitude compatible with the Froissart constraint.<sup>25</sup>

The existing data do not supply us with information to determine definitely the asymptotic mode of the scattering amplitude. Though in a number of papers<sup>12, 15, 22</sup>

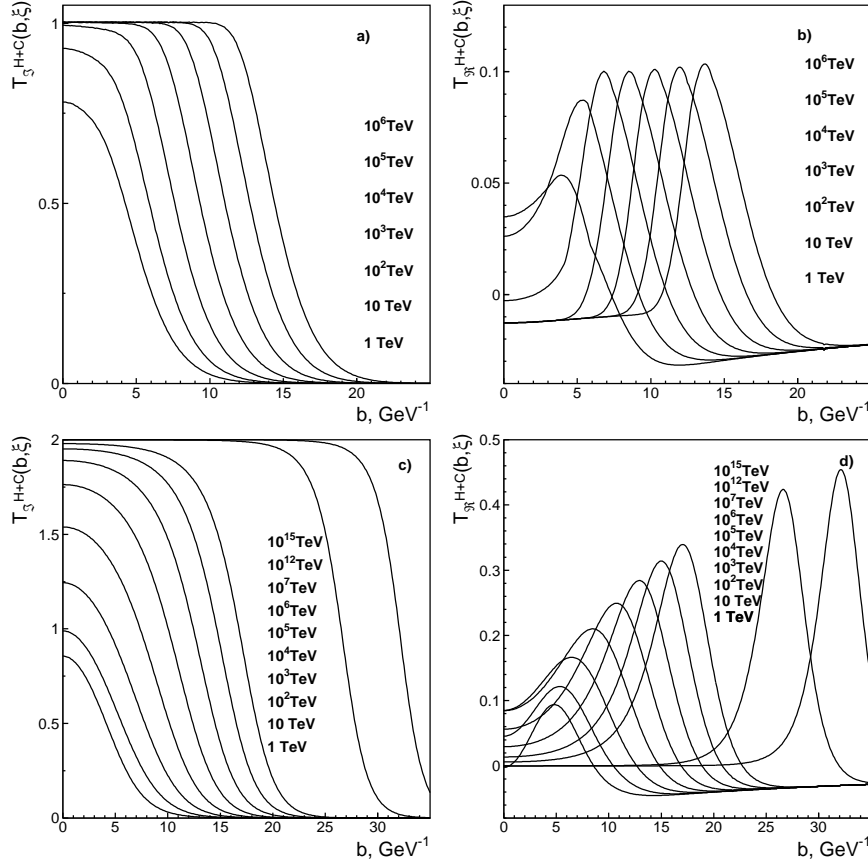


Fig. 5. Profile functions (imaginary and real parts) in the energy region  $\sqrt{s} = 1 - 10^6$  TeV with the Coulomb interaction taken into account; (a,b) refer to the black disk mode, (c,d) to the resonant disk mode.

the appearance of a black spot at LHC energy in the profile function at small  $b$  is emphasized, one can not come to a definite conclusion.

In both modes at small  $\mathbf{q}^2$  the imaginary parts of the amplitudes dominate over the real parts, namely,  $A_{\mathbb{S}}^H(\mathbf{q}^2, \ln s) \sim \ln^2 s$  while  $A_{\mathbb{R}}^H(\mathbf{q}^2, \ln s) \sim \ln s$ . The Coulomb and hadronic interaction interplay is realized due to the interference in the real part of the amplitude. In that case the real part of the resonant disk amplitude is essentially larger than that for the black disk mode. In the  $pp$  scattering the large interference is realized in a shoulder in the region  $\mathbf{q}^2 \sim 0.0025 - 0.0075$  GeV<sup>2</sup> (see Fig. 6).

We see the data are sensitive to the formation of the resonant disk mode. The interference effects provide a possibility to find arguments for or against of switching-on the resonant disk regime.

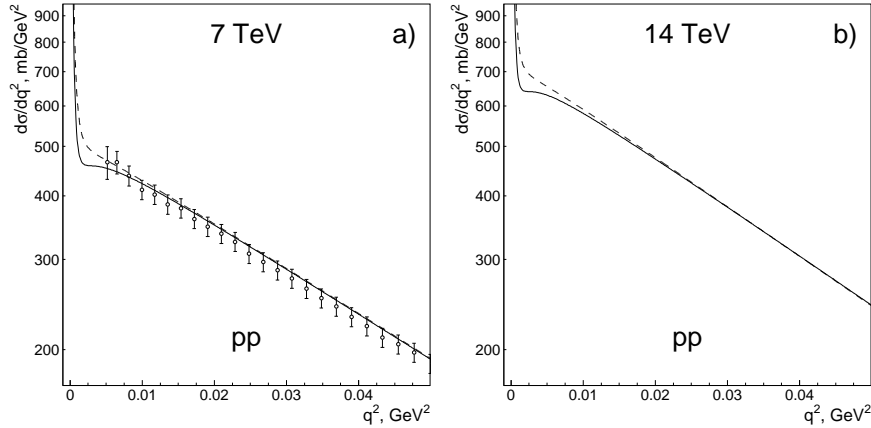


Fig. 6. Diffractive scattering cross sections for  $pp$  at 7 TeV (a) and at 14 TeV (b) (Eq. (10),  $\lambda=0.01$  GeV). The dashed line refers to the black disk mode and the solid one to the resonant disk mode.

#### Acknowledgement

We thank Y.I. Azimov and A.V. Sarantsev for useful discussions. The work was supported by RSGSS-4801.2012.2 grant.

#### References

1. G. Arnison *et al.* [UA1 Collaboration], Phys. Lett. B **128**, 336 (1983).
2. M. Bozzo *et al.* [UA4 Collaboration], Phys. Lett. B **147**, 385 (1984).
3. N. A. Amos *et al.* [E-710 Collaboration], Phys. Lett. B **247**, 127 (1990).
4. C. Augier *et al.* [UA4/2 Collaboration], Phys. Lett. B **316**, 448 (1993).
5. F. Abe *et al.* [CDF Collaboration], Phys. Rev. D **50**, 5518 (1994).
6. G. Latino [on behalf of TOTEM Collaboration], EPJ Web Conf. **49**, 02005 (2013).
7. G. Aad *et al.* [ATLAS Collaboration], Eur. Phys. J. C **72**, 1926 (2012).
8. V. Khachatryan *et al.* [CMS Collaboration], Phys. Rev. D **92**, 012003 (2015).
9. B. Abelev *et al.* [ALICE Collaboration], Eur. Phys. J. C **73**, 2456 (2013).
10. M.L. Good and W.D. Walker, Phys. Rev. **120**, 1857 (1960).
11. L. G. Dakhno and V. A. Nikonov, Eur. Phys. J. A **5**, 209 (1999).
12. M.M. Block and F. Halzen, Phys. Rev. **D86**, 0501504 (2013).
13. V.V. Anisovich, V.A. Nikonov and J. Nyiri, Phys. Rev. D **88**, 094015 (2013).
14. S.M. Troshin and N.E. Tyurin, Int. J. Mod. Phys. A **29**, 1450151 (2014).
15. I.M. Dremin, Bull. Lebedev Phys. Inst. **42**, 21 (2015) [Kratk. Soobshch. Fiz. **42**, 8 (2015)] [arXiv:1404.4142 [hep-ph]].
16. V.V. Anisovich, V.A. Nikonov and J. Nyiri, Phys. Rev. D **90**, 074005 (2014).
17. T.K. Gaisser and T. Stanev, Phys. Lett. B **219**, 375 (1989).
18. M.M. Block, F. Halzen and B. Margolis, Phys. Lett. B **252**, 481 (1990).
19. R.S. Fletcher, Phys. Rev. D **46**, 187 (1992).
20. V.V. Anisovich, V.M. Shekhter, Sov. J. Nucl. Phys. **28**, 561 (1978); [Yad. Fiz. **28**, 1079 (1978)].
21. V.V. Anisovich, E.M. Levin, M.G. Ryskin, Sov. J. Nucl. Phys. **29**, 674 (1979); [Yad. Fiz. **29**, 1311 (1979)].

22. V.V. Anisovich, K.V. Nikonov and V.A. Nikonov, Phys. Rev. D **88**, 014039 (2013).
23. V.V. Anisovich, V. A. Nikonov and J. Nyiri, Int. J. Mod. Phys. A **29**, 1450096 (2014).
24. V.V. Anisovich, Phys. Usp. **58**, 963 (2015); [UFN **185**, 1043 (2015)].
25. M. Froissart, Phys. Rev. **123**, 1053 (1961).
26. V.V. Anisovich, V. A. Nikonov and J. Nyiri, arXiv:1508.02140 [hep-ph].
27. V.V. Anisovich, V.A. Nikonov and J. Nyiri, Int. J. Mod. Phys. A **30**, 1550188 (2015).
28. V. V. Anisovich and V. A. Nikonov, arXiv:1601.07015 [hep-ph] (will be published in Mod. Phys. Lett. A).
29. H.A. Bethe, Annals Phys. **3**, 190 (1958).
30. L.D. Soloviev, Zh. Exp. Theor. Fiz. **49**, 292 (1966) [Sov. Phys. JETP **22**, 205 (1966)].
31. G.B. West and D. R. Yennie, Phys. Rev. **172**, 1413 (1968).
32. V. Franco, Phys. Rev. D **7**, 215 (1973).
33. R. Cahn, Z. Phys. C **15**, 253 (1982).
34. V. Kundrat and M. Lokajicek, Z. Phys. C **63**, 619 (1994).
35. J. Kaspar, V. Kundrat, M. Lokajicek and J. Prochazka, Nucl. Phys. B **843**, 84 (2011).
36. E. Martynov, arXiv:1412.0269[hep-ph].
37. F. Nemes, T. Csörgő and M. Csanád, Int. J. Mod. Phys. A **30** 1550076 (2015).
38. M. Giordano and E. Megiolaro, Phys. Lett. B **744**, 263 (2015).
39. I.M. Dremin, Adv. High Energy Phys. 2015, 912743 (2015).
40. I.M. Dremin, Phys. Usp. **58**, 61 (2015); [UFN **185**, 65 (2015)].
41. S.M. Troshin and N.E. Tyurin, arXiv:1601/00483 [hep-ph].
42. V.N. Gribov, Sov. J. Nucl. Phys. **17**, 313 (1973).